Converged AC Power Flow Cases from Linear Production Cost Models via ACOPF

Eran Schweitzer, Brent Eldridge, Michael Abdelmalak, Nader Samaan
Pacific Northwest National Laboratory

***Abstract*—This paper demonstrates the efficacy of using AC optimal power flow (ACOPF) to obtain multiple, converged AC power flow (ACPF) cases from production cost model (PCM) solutions. The scarcity of reliable methods to obtain converged ACPF cases from dispatch models has become a critical limiting factor in the effort to increase the number of study scenarios in long-term transmission planning studies. Long-term planning scenarios often vary substantially from today's system in terms of network topology, resource mix, and load profiles. As a result, developing converged ACPF cases from closely matching initial starting points is not a viable path. The proposed method modifies the standard ACOPF model to determine an initial voltage profile, reactive power dispatch, and new reactive shunt additions to initialize a more detailed ACPF model. Results are demonstrated on 20 snapshots of the 2030 Western Electricity Coordinating Council (WECC) Anchor Data Set (ADS) with approximately 27,900 branches.**

***Index Terms*—power system simulation, optimal power flow**

I. Introduction

Given recent increases in electricity demand and rapid technological and structural changes to the electric grid, the number of scenarios that must be considered during transmission planning is increasing. Federal Energy Regulatory Commission (FERC) Order 1920 [1] requires a minimum of three long-term scenarios, with power flow snapshots used to capture operating conditions for each scenario. The New York Independent System Operator (NYISO), for example, develops 12 cases per scenario—3 years of summer, winter, spring, and light-load—for a total of 36 power flow cases [2]. Production cost models (PCMs) are a natural choice to determine system operating points, and there are industry efforts in this direction [3]. While there have been improvements in AC solutions to the multi-period unit commitment problem, robust solutions for long simulations are still in the research and development phase [4]. PCMs, therefore, use linearized power flow representations and require effort to convert their results to converged AC power flow (ACPF) solutions.

The chronological AC power flow automated generation tool (C-PAGE) [5] was developed to help move from PCM to ACPF. It has been used to develop future, converged ACPF cases with different topology and resource mixes compared to today's system [6], [7]. While C-PAGE performs well in finding sequential AC solutions from an initial converged case, finding this initial ACPF case has frequently required a time-intensive manual process. This paper addresses this gap by developing an AC optimal power flow (ACOPF) approach to consistently and robustly reach a converged ACPF solution that matches the economic dispatch from the PCM.

The Pacific Northwest National Laboratory is operated for the U.S. Department of Energy (DOE) by the Battelle Memorial Institute under Contract DE-AC05-76RL01830.
corresponding author: Eran Schweitzer (eran.schweitzer@pnnl.gov)

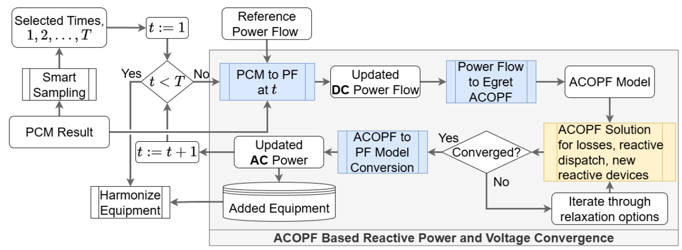

Fig. 1. Analysis pipeline from PCM to AC power flow over snapshots, data conversion steps (blue), and ACOPF solution step (yellow).

II. Solution Approach

The AC convergence process described in this paper is part of an analysis pipeline depicted in Fig. 1. A subset of PCM snapshots are sampled from representative hours [8]. Each snapshot is first converted to a DC power flow (DCPF) case, which manages modeling differences between the PCM and power flow domains.

To convert this DCPF case into an ACPF solution, the main contribution of this paper, an ACOPF model is generated from the DCPF snapshot using a modified version of the ACOPF model in EGRET [9]. This model maintains generator dispatch, adjusts for any losses not accounted for in linearized formulations, determines the reactive power dispatch, and places additional reactive shunts to develop a feasible AC solution. The ACOPF solution is then converted to ACPF, where simplifying assumptions, such as continuous treatment of controls, are replaced with more detailed models.

III. Model Translations

Several translations, highlighted in blue in Fig. 1, are necessary to move between tools.

A. PCM to DC Power Flow

Although PCM generally uses the same system equations as DCPF, loads, generators, and high voltage DC (HVDC) are often modeled at different levels of detail.

979-8-3315-8138-1

1) Distributed Injections: PCM inputs typically specify load at a regional level. Additionally, behind-the-meter and demand response resources are modeled separately in PCMs, but often lumped into the bus load objects in the power flow. Generators in PCM, often aggregate multiple units into a single plant, or map several small interconnection points into a single injection. PCM outputs are mapped from their aggregated representation to individual injections using predefined distribution factors. The disaggregated values are used as input to the power flow model.

2) Specialized Mapping: Generator step-up transformers or more complex collector systems may be neglected in the PCM. Some point-to-point lines in the PCM are modeled as multi-terminal HVDC (MTDC) in power flow models, and therefore, as a set of converters. A list of these instances is maintained, and they are mapped to distribute PCM data to the appropriate location in the power flow.

3) HVDC Modeling: Integration of HVDC models into power flow tools, especially MTDC, remains an active area of research [10]. As a result, HVDC treatment is more tool specific. Most power flow models of point-to-point HVDC lines, fix the rectifier and inverter terminals, thus fixing the flow direction. Each HVDC line in the power flow model therefore is duplicated to have a version that can flow in each direction. The appropriate instance is activated based on the PCM result, and flow mapped to the rectifier.

B. DCPF to ACOPF

Simplifications to DCPF data that are passed to the ACOPF model are briefly described below.

1) Shunts: Nearly all reactive shunts (i.e., line shunts, fixed bus shunts, switched bus shunts, and variable bus shunts) are set in service and converted to continuous variable shunts to provide the widest possible feasible space to the ACOPF model. Shunts with real admittance components—most notably in the Western Electricity Coordinating Council (WECC), the Chief Joe Brake—are the exception and are not modified, so that resistive loads are not altered.

2) HVDC: Reactive power consumption is estimated from the rectifier and inverter equations [11]. The DC current is solved for based on the real power from the PCM, and $1\,\mathrm{p.u.}$ voltage magnitude, from which the reactive power estimate can be calculated. Similarly, estimates of losses are based on assumed power transfer and line resistance.

3) MTDC: Each MTDC converter injection is fixed and modeled individually as a load using the same rectifier and inverter equations described in the previous section.

C. ACOPF to ACPF

This step extracts needed information from the ACOPF and applies it to a ACPF tool to drive Newton-Raphson convergence to a high-voltage solution.

1) Voltage Setpoints: The ACOPF voltage magnitude solution is used to update any regulated voltage set points. This ensures that any outer control loops, or PV buses, do not push the solution away from the ACOPF solution.

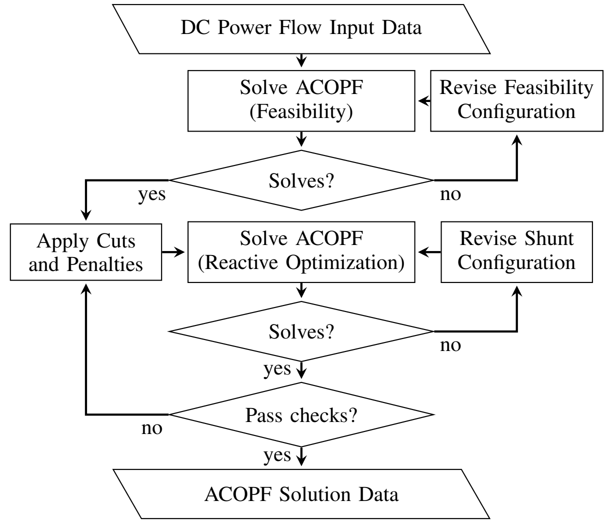

Fig. 2. ACOPF Solution Stages (yellow process in Fig. 1).

2) Pre-existing shunts: Continuous variable shunt devices, such as static VAR compensators, can be mapped directly. The remaining models are converted back to their original representation. For fixed shunts, including line shunts, a rounding approach is used to determine whether the device is connected or disconnected. For discrete switched shunts, such as capacitor banks, that have one or more steps, the ACOPF solution value is rounded to nearest viable step.

3) New shunts: All new reactive support devices added through ACOPF currently are modeled as discrete shunt components with ratings equal to the ACOPF solution.

4) HVDC converter reactive compensation: The updated voltage magnitudes from the ACOPF yield updated reactive power consumption from those in III-B. Where needed, the difference between actual and initial converter reactive power consumption is compensated by adding shunt components at converter terminals.

5) Solution settings: In this work, all control settings (such as transformer tap changers, switched shunts, and distributed slacks) are disabled to ensure the ACPF solver has the least deviation from the given ACOPF solution. Future work will incorporate these additional controls.

IV. Modified ACOPF

The following section describes the ACOPF solution process, illustrated in Fig. 2. The general model formulation is described in Sec. IV-A. The first stage, described in Sec. IV-B, rapidly generates a feasible solution to be further refined in subsequent solves. The second stage, described in Sec. IV-C, solves a reactive power dispatch problem, during which any shunt additions are minimized. Sec. IV-D checks the solution before passing to the detailed ACPF model.

A. Model Constraints

For brevity, this section presents only the constraints that are added or modified from the standard polar squared voltage ACOPF model formulation [12].

Generator bounds are given an upper limit equal to the PCM dispatch solution, P_g^*, and a lower limit of zero. Generator

979-8-3315-8138-1

dispatch is then given a negative marginal cost, $C_g < 0$, to discourage deviation from the PCM solution.

$$c_g^{\text{gen}} = C_g^{\text{gen}} p_g, \quad \forall g \in \mathcal{G} \tag{1a}$$
$$0 \le p_g \le P_g^*, \quad \forall g \in \mathcal{G} \tag{1b}$$

PCM load data account for line losses, which is a common industry practice [13]. Because the ACOPF endogenously includes losses, we allow area-wide line-loss adjustments. *Load curtail proxy* generators, $i \in \mathcal{N}^{\text{lcp}}$, are added at each conforming load bus, partitioned into areas $a \in \mathcal{A}$, where $\mathcal{N}_a^{\text{lcp}}$ denotes the buses in area a. To minimize the adjustment, each proxy p_i^{lcp} is given a curtailment marginal cost $C_i^{\text{lcp}} > 0$.

$$c_i^{\text{lcp}} = C_i^{\text{lcp}} p_i^{\text{lcp}}, \quad \forall i \in \mathcal{N}^{\text{lcp}} \tag{2a}$$
$$0 \le p_i^{\text{lcp}} \le D_i, \quad \forall i \in \mathcal{N}^{\text{lcp}} \tag{2b}$$
$$p_i^{\text{lcp}} = \eta_a^{\text{lcp}} D_i^{\text{p}}, \quad \forall a \in \mathcal{A}, i \in \mathcal{N}_a^{\text{lcp}} \tag{2c}$$
$$0 \le \eta_a^{\text{lcp}} \le 1, \quad \forall a \in \mathcal{A} \tag{2d}$$
$$D_i^{\text{p}} q_i^{\text{lcp}} = D_i^{\text{q}} p_i^{\text{lcp}}, \quad \forall i \in \mathcal{N}^{\text{lcp}}. \tag{2e}$$

Where D_i^{p} and D_i^{q} are the real and reactive load at bus i, η_a^{lcp} is a variable for the relative load curtailment in area a, and (2e) maintains a constant power factor.

To ensure AC feasibility, new shunt devices are allowed to be placed at all load or load neighbor buses, and all generator or generator neighbor buses with nominal voltage $V^{\text{nom}} \ge 100$ kV, denoted by $i \in \mathcal{N}^{\text{ssp}}$. These *slack shunt proxy* generators are given a large upper bound for reactive power injection (negative for withdrawal) and zero real power capability. As with load curtailment, shunt proxies $q_i^{\text{ssp+}}$ and $q_i^{\text{ssp-}}$ are given a marginal cost C_i^{ssp} to discourage addition:

$$c_i^{\text{ssp}} = C_i^{\text{ssp}}(q_i^{\text{ssp+}} - q_i^{\text{ssp-}}), \quad \forall i \in \mathcal{N}^{\text{ssp}} \tag{3a}$$
$$-Q_i^{\text{ssp}} \le q_i^{\text{ssp-}} \le 0 \le q_i^{\text{ssp+}} \le Q_i^{\text{ssp}}, \quad \forall i \in \mathcal{N}^{\text{ssp}} \tag{3b}$$
$$p_i^{\text{ssp}} = 0. \quad \forall i \in \mathcal{N}^{\text{ssp}} \tag{3c}$$

Voltage magnitude limits are applied to each bus $i \in \mathcal{N}^{\text{reg}}$ that has voltage regulation bounds, $(V_i^{\min}, V_i^{\max})$, and is on the high-voltage network, $V_i^{\text{nom}} \ge 100$ kV. Relaxed limits, $\hat{V}_i^{\min}$ and $\hat{V}_i^{\max}$, represent an extreme range that is only expected to occur rarely, if ever. Buses in $\mathcal{N}^{\text{reg}}$ can violate their bounds at a nonlinear quadratic total cost, c_i^{vm}, up to these relaxed limits. All remaining buses (i.e., unregulated or under 100 kV) are given the relaxed limits.

$$\begin{aligned} c_i^{\text{vm}} = {} & C_{1,i}^{\text{vm}}(v_i^- + v_i^+) \\ & + C_{2,i}^{\text{vm+}}(v_i^+)^2 + C_{2,i}^{\text{vm-}}(v_i^-)^2, \quad \forall i \in \mathcal{N}^{\text{reg}} \end{aligned} \tag{4a}$$
$$\hat{V}_i^{\min} \le v_i \le \hat{V}_i^{\max}, \quad \forall i \in \mathcal{N} \tag{4b}$$
$$v_i + v_i^- \ge V_i^{\min}, \quad \forall i \in \mathcal{N}^{\text{reg}} \tag{4c}$$
$$v_i - v_i^+ \le V_i^{\max}, \quad \forall i \in \mathcal{N}^{\text{reg}} \tag{4d}$$
$$v_i^+, v_i^- \ge 0, \quad \forall i \in \mathcal{N}^{\text{reg}} \tag{4e}$$

where $C_{1,i}^{\text{vm}}$, $C_{2,i}^{\text{vm+}}$, and $C_{2,i}^{\text{vm-}}$, are determined by a nominal marginal cost C^{vm} and scalar $\alpha^{\text{vm}} > 0$.

$$C_{1,i}^{\text{vm}} = C^{\text{vm}} V_i^{\text{nom}}, \quad \forall i \in \mathcal{N}^{\text{reg}} \tag{5a}$$
$$C_{2,i}^{+} = \frac{\alpha^{\text{vm}} C_{1,i}^{\text{vm}}}{2(\hat{V}_i^{\max} - V_i^{\max})}, \quad \forall i \in \mathcal{N}^{\text{reg}} \tag{5b}$$
$$C_{2,i}^{-} = \frac{\alpha^{\text{vm}} C_{1,i}^{\text{vm}}}{2(V_i^{\min} - \hat{V}_i^{\min})}, \quad \forall i \in \mathcal{N}^{\text{reg}}. \tag{5c}$$

The marginal cost C^{vm}, in \$/kV, imposes larger violation penalties in higher voltage systems. The parameters $C_{1,i}^{\text{vm}}, C_{2,i}^{+}$, and $C_{2,i}^{-}$ are then converted to per unit and formulated such that the derivative of the quadratic terms in (4a) is at most α^{vm} times larger than the linear marginal cost $C_{1,i}^{\text{vm}}$.

Point-to-point HVDC lines are modeled as two *DC proxy* generators, $(i, j, k) \in \mathcal{K}^{\text{dcp}}$, with coupling constraints to model losses and point-to-point service from bus i to j on branch k. As described in Sec. III-B, converter injections P_{ijk}^{dc} and P_{jik}^{dc} for HVDC branch k from i to j are provided. These are used to calculate a marginal loss term L_k:

$$L_k := \frac{P_{ijk}^{\text{dc}} + P_{ijk}^{\text{dc}}}{\min(P_{ijk}^{\text{dc}}, P_{jik}^{\text{dc}})}, \quad \forall (i, j, k) \in \mathcal{K}^{\text{dcp}}. \tag{6}$$

Proxy generation marginal cost $C_i^{\text{dcp}} < 0$ penalizes dispatch away from the branch's PCM setpoints. Reactive setpoints are fixed, as described in Sec. III-B. Each HVDC line is then modeled as follows, where i' and j' denote the actual flow direction, that is, such that $P_{i'j'k}^{\text{dc}} < 0$.

$$c_{i'}^{\text{dcp}} = C_{i'}^{\text{dcp}} p_{i'}^{\text{dcp}}, \quad \forall (i', j', k) \in \mathcal{K}^{\text{dcp}} \tag{7a}$$
$$(1 - L_k) p_{i'}^{\text{dcp}} + p_{j'}^{\text{dcp}} = 0, \quad \forall (i', j', k) \in \mathcal{K}^{\text{dcp}} \tag{7b}$$
$$P_{i'j'k}^{\text{dc}} \le p_{i'}^{\text{dcp}} \le 0 \le p_{j'}^{\text{dcp}} \le P_{j'i'k}^{\text{dc}}, \quad \forall (i', j', k) \in \mathcal{K}^{\text{dcp}} \tag{7c}$$
$$q_{i'}^{\text{dcp}} = Q_{i'j'k}^{\text{dc}}, \quad q_{j'}^{\text{dcp}} = Q_{j'i'k}^{\text{dc}}, \quad \forall (i', j', k) \in \mathcal{K}^{\text{dcp}} \tag{7d}$$

Existing variable shunts are also modeled as proxy generators. An outer-approximation is used to determine reactive bounds from the minimum and maximum shunt settings, and real power output is fixed at zero. Implementing variable shunts via a continuous cubic term, $b_i v_i^2$, presented convergence difficulties during implementation tests.

The ACOPF objective function typically minimizes generator production costs. For the purposes of generating an initial ACPF solution matching PCM dispatch, all production costs are removed from the objective function and replaced with total costs from equations (1a), (2a), (3a), (4a), and (7a).

$$\begin{aligned} \min z = {} & \sum_{g \in \mathcal{G}} c_g^{\text{gen}} + \sum_{i \in \mathcal{N}^{\text{lcp}}} c_i^{\text{lcp}} + \sum_{i \in \mathcal{N}^{\text{ssp}}} c_i^{\text{ssp}} \\ & + \sum_{i \in \mathcal{N}^{\text{reg}}} c_i^{\text{vm}} + \sum_{(i', j', k) \in \mathcal{K}^{\text{dcp}}} c_{i'}^{\text{dcp}}. \end{aligned} \tag{8}$$

B. Feasibility

As described in Sec. IV-A and highlighted in (8), the ACOPF formulation contains many, possibly conflicting, objectives. This implementation allows flexibility in solving the model in multiple stages, first emphasizing model feasibility before optimizing reactive shunt additions.

Input parameters are summarized in Table I. Generators and DC branch proxies both have a cost of -\$2,000/MW to encourage dispatch at PCM levels, and load curtail proxies have a cost of \$2,000/MW to discourage unnecessary load curtailment. Voltage magnitude bounds are relaxed to $\pm 25\%$ and penalized at \$1,000/kV. Finally, the set of slack shunt proxy generators is extended to all network buses, $\mathcal{N}^{\text{ssp}} = \mathcal{N}$.

979-8-3315-8138-1

TABLE I
ACOPF PARAMETERS

Symbol	Description	Feas.	Q-Opt.	Units
$\hat{V}_i^{\min}$	Relaxed min. voltage mag.	0.75	0.75	p.u.
$\hat{V}_i^{\max}$	Relaxed max. voltage mag.	1.25	1.25	p.u.
C_g^{gen}	Generator dispatch cost	-2000	-2000	$/MW
C_i^{lcp}	Load curtail proxy cost	2000	0	$/MW
C_i^{ssp}	Slack shunt proxy cost	0	500	$/Mvar
C^{vm}	Voltage violation penalty	1000	1000	$/kV
α^{vm}	Quadratic penalty scalar	10	10	None
C_i^{dcp}	DC proxy generator cost	-2000	-2000	$/MW
μ	Std. dev. perturbation to C_i^{ssp}	0	10^{-3}	$/MW

To improve solver performance, all variable values are initialized to be in the interior of the formulation's feasible region. In addition, primal, dual, and complementarity optimality tolerances are increased to 10^{-3}, because the solution will be further refined in the second stage. Adjustments and fine tuning for these configurations could be made, as shown in Fig. 2, but results in Sec. V show that all cases were solvable using the initial configurations.

C. Reactive Optimization

The second stage refines the solution by identifying sparser reactive support, higher quality voltage profile, and further reducing the adjustments for line losses. As shown in Table I the load curtailment cost is changed to zero, and the shunt proxy cost is increased to \$500/Mvar. The first stage solution is used as an initial solution in the second stage. However, using $\mathcal{N}^{\text{ssp}} = \mathcal{N}$ might include reactive injections at buses that do not match the intended $\mathcal{N}^{\text{ssp}}$ definition of Sec. IV-A. To account for this, all proxy shunts at buses $i \in \mathcal{N} \setminus \mathcal{N}^{\text{ssp}}$ are given an additional penalty cost and new upper bounds from the first stage solution. To avoid exceeding the first stage load adjustments, load curtail proxies are also given new upper bounds, replacing the upper bound in (2b) with P_i^{lcp} from the first stage solution. To avoid degeneracy and numerical instability given the many possible shunt locations, a small perturbation is added to the shunt proxy marginal cost, $\hat{C}_i^{\text{ssp}} = C_i^{\text{ssp}} + N(0, \mu)$.

D. Solution Quality

Checks are conducted before the ACOPF solution is sent for ACPF analysis. These ensure that all generators and DC branch proxies match the PCM solution, reactive shunts are only added at appropriate buses, the total line loss adjustment is less than 10%, and there are no more than 100 voltage magnitude violations greater than 0.05 p.u. at regulated buses.

V. USE CASES

In the examples presented, the PCM outputs come from GridView [14], the format WECC uses to produce the bi-annual Anchor Data Set (ADS) [15], DCPF and ACPF use PowerWorld [16]. The ACOPF is implemented in EGRET [9] and solved using Ipopt [17] version 3.14.19 with MUMPS 5.8.1 on a 3.20 GHz processor with 64GB RAM. The WECC ADS model has approximately 23,600 buses, 27,900 branches, 3,600 generators, and 3,800 shunt devices [18].

TABLE II
SUMMARY OF ACOPF SOLVE TIMES AND RESULTS

Case	Solve Time (min)			Addl.	Loss
(yy-mm-dd hb)	Feas.	Q-Opt.	Total	Shunts	Adj.
2030-01-03 21	1.51	6.06	7.88	99	4.33%
2030-01-07 14	1.49	11.79	13.59	95	4.98%
2030-01-15 23	1.51	4.81	6.64	98	4.55%
2030-01-21 08	1.52	12.14	13.96	99	4.40%
2030-01-28 16	2.38	13.51	16.21	97	4.39%
2030-04-07 12	4.00	15.78	20.09	118	5.19%
2030-04-07 13	14.02	17.21	31.54	115	5.20%
2030-04-07 14	4.17	20.25	24.72	112	5.20%
2030-04-07 15	3.97	11.72	16.00	114	5.15%
2030-04-14 13	5.52	18.38	24.21	103	6.26%
2030-04-14 14	5.09	14.08	19.48	104	6.23%
2030-07-19 17	1.60	20.60	22.51	78	3.37%
2030-07-29 17	1.49	12.95	14.75	81	3.28%
2030-07-29 18	1.47	14.81	16.59	79	3.18%
2030-07-29 19	1.51	6.05	7.89	77	3.22%
2030-10-07 18	2.45	21.98	24.75	84	3.73%
2030-10-15 05	2.76	17.35	20.43	82	4.42%
2030-10-21 12	4.24	15.95	20.50	81	4.08%
2030-10-28 08	1.48	4.01	5.80	98	4.69%
2030-10-31 23	1.92	20.29	22.52	83	5.45%

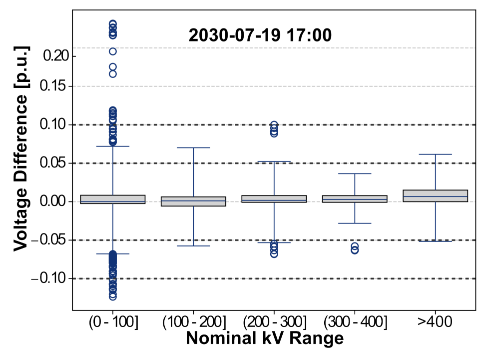

Fig. 3. Voltage magnitude difference between EGRET and PowerWorld.

A. ACOPF Solutions

Results from the two-stage ACOPF solution process are shown in Table II, using parameter values from in Table I. The number of added shunts and loss adjustments both show clear seasonality, with the most shunt additions and the largest loss adjustments in the spring cases, while the summer cases show the fewest shunt additions and lowest loss adjustments. All loss adjustments are relatively consistent and within an expected range around 5% [19]. Future work will focus on identifying a single set of planned shunt additions for all cases.

B. ACPF Validation

A key role of ACOPF is to provide a good initialization to the Newton-Raphson algorithm. It is therefore useful to consider the similarity of the ACOPF and ACPF solutions. Fig. 3 shows the voltage magnitude difference by voltage level between the two solutions. Most of the buses show minimal deviations, suggesting that the solutions largely align.

Fig. 4 shows voltage distribution by kV-level for three snapshots throughout the year. Most voltages lie within the expected range. A few more extreme values are seen below 100 kV; however, model data in this part of the system are less reliable, are generally not considered as closely in studies

979-8-3315-8138-1

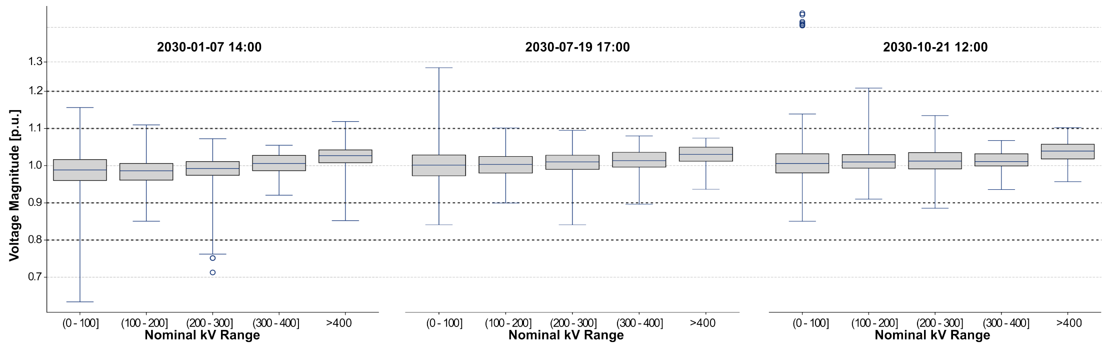

Fig. 4. Bus voltage magnitude per kv-level in PowerWorld for several converged snapshots.

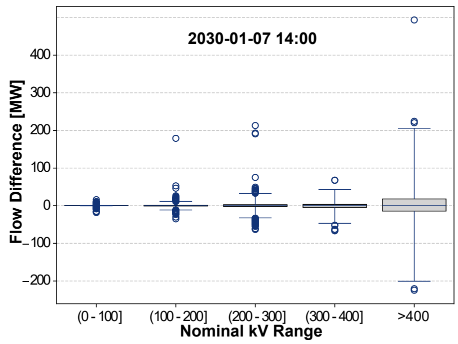

Fig. 5. Flow comparison between DCPF input and converged ACPF.

using the full interconnection model, and with few exceptions are not considered part of the bulk electric system [20]. Finally, Fig. 5 compares flows from the input DCPF case, which in turn come from the PCM, to those in the converged ACPF case. Once again, most of the flows show little deviation, which indicates that the operating snapshot from the PCM has been preserved in the ACPF solution.

VI. Conclusion

Long-term planning studies often include numerous changes to network topology, resource mix, and load profiles, requiring significant effort to develop converged ACPF. This study demonstrates how PCM solutions can be reliably translated across DCPF, ACOPF, and ACPF models to overcome this challenge and thus enable an increase in study scenarios, as required by FERC Order 1920. Mismatches emerge at each stage due to differences in model granularity, but we show that such errors are minimal and easily compensated in the final converged ACPF solutions. Future work will focus on harmonizing the set of shunt additions across planning cases. This step is critical for practical application in planning contexts, as practical implementations must rely on a single, unified set of network improvements.

References

[1] FERC, "Order No. 1920: Building for the future through electric regional transmission planning and cost allocation and generator interconnection," Docket No. RM21-17-000. [Online]. Available: https://www.ferc.gov/media/e1-rm21-17-000

[2] K. Burrell, "Overview of the coordinated grid planning process," Aug. 2024, New York ISO: TPAS/ESPWG. [Online]. Available: https://www.nyiso.com/documents/20142/46217988/06a_2024_CGPP_Update_ESPWG_20240806_vFinal.pdf

[3] WECC, "Round-trip fact sheet," Jul. 2024. [Online]. Available: https://www.wecc.org/wecc-document/3556

[4] J. T. Holzer *et al.*, "GO competition challenge 3: Problem, solvers, and solution analysis," 2024. [Online]. Available: https://arxiv.org/abs/2411.12033

[5] B. Vyakaranam *et al.*, "Automated tool to create chronological AC power flow cases for large interconnected systems," *IEEE Open Access Journal of Power and Energy*, vol. 8, pp. 166–174, 2021.

[6] U.S. Department of Energy, Grid Deployment Office, "The National Transmission Planning Study," 2024, Washington, D.C.: U.S. Department of Energy. [Online]. Available: https://www.energy.gov/gdo/national-transmission-planning-study

[7] T. C. Douville *et al.*, "West coast offshore wind transmission study," Tech. Rep., 01 2025. [Online]. Available: https://www.osti.gov/biblio/2500279

[8] T.-C. Chen *et al.*, "Smart sampling of representative hourly power generation scenario with high renewable penetration," *IEEE Access*, vol. 12, pp. 115 319–115 328, 2024.

[9] "EGRET," https://github.com/grid-parity-exchange/Egret.

[10] Q. H. Nguyen *et al.*, "Review of modeling gaps and a solution for AC-MTDC power flow in commercial tools," in *2025 IEEE Power & Energy Society General Meeting (PESGM)*, 2025.

[11] PowerWorld Corporation, "Rectifier and Inverter Model." [Online]. Available: https://www.powerworld.com/WebHelp/Default.htm#MainDocumentation_HTML/DC_Line_Options_Rectifier_Parameters.htm

[12] M. B. Cain *et al.*, "History of optimal power flow and formulations," Federal Energy Regulatory Commission, 2012. [Online]. Available: https://www.ferc.gov/sites/default/files/2020-05/acopf-1-history-formulation-testing.pdf

[13] T. J. Overbye *et al.*, "A comparison of the AC and DC power flow models for LMP calculations," in *Proceedings of the 37th Annual Hawaii international conference on system sciences*. IEEE, 2004.

[14] Hitachi Energy, "GridView: Integrated engineering and economic analysis of the electric power grid." [Online]. Available: https://www.hitachienergy.com/us/en/products-and-solutions/energy-portfolio-management/enterprise/gridview

[15] WECC, "Anchor Data Set (ADS)." [Online]. Available: https://www.wecc.org/program-areas/reliability-planning-performance-analysis/reliability-modeling/anchor-data-set-ads

[16] PowerWorld Corporation, "PowerWorld Simulator." [Online]. Available: https://www.powerworld.com/products/simulator/overview

[17] A. Wächter and L. T. Biegler, "On the implementation of an interior-point filter line-search algorithm for large-scale nonlinear programming," *Mathematical programming*, vol. 106, no. 1, pp. 25–57, 2006.

[18] K. Oikonomou *et al.*, "Western interconnection baseline study," Tech. Rep., 09 2024, Pacific Northwest National Laboratory (PNNL), Richland, WA (United States). [Online]. Available: https://www.osti.gov/biblio/2440740

[19] L. Wong, "A review of transmission losses in planning studies," California Energy Commission, Tech. Rep., Aug. 2011, DOCKET 11-IEP-1C. [Online]. Available: https://efiling.energy.ca.gov/GetDocument.aspx?tn=62058

[20] NERC, "Glossary of Terms Used in NERC Reliability Standards." [Online]. Available: https://www.nerc.com/pa/stand/glossaryofterms/glossary_of_terms.pdf

979-8-3315-8138-1